VER
Vascular & Endovascular Review

A Deep Learning System For The Automated Detection And Segmentation Of Abdominal Aortic Aneurysm From Computed Tomography Angiography

[1*] Dr.Shubhashree Sahoo, [1]G.B.Hima Bindu, [2]Dr.T.Vengatesh, [3]P.Boomi, [4]Dr. Seetha J, [5]Dr.Prajwalasimha S N, [6]Saint Jesudoss.S, [7]Dhananjay Shripad Rakshe

[1*](Coressponding Author) Assistant professor, CSE (AI&ML), Sphoorthy engineering college Nadargul, Hyderabad-501510, India. Email ID: shubhashree@sphoorthyengg.ac.in
[1]Associate Professor, Department of Computer Science and Engineering, School of Technology, The Apollo University, The Apollo Knowledge City, Saketa, Murukambattu, Chittoor - 517127, Andhra Pradesh , India. Email ID: himabindugbe@gmail.com
[2]Assistant Professor, Department of Computer Science, Government Arts and Science College, Veerapandi, Theni, Tamilnadu, India. Email ID: venkibiotinix@gmail.com
[3]Assistant Professor,Department of Mathematics,V.S.B Engineering College(Autonomous), Karur, Tamilnadu, India. Email ID : rpboomi@gmail.com
[4]Professor / CSBS, Department of Computer Science and Business Systems, Panimalar Engineering College , Chennai, Tamilnadu, India. Email ID:jsvpec@gmail.com
[5]Department of Computer Science and Engineering (Cyber Security), School of Engineering (SoE), Dayananda Sagar University, Bangalore, India, Email ID: prajwalasimha.sn1@gmail.com
[6]Assistant Professor, Department of Computer Science and Engineering, Rajiv Gandhi College of Engineering and Technology, Puducherry, India. Email ID : saint.2k5@gmail.com
[7] Assistant Professor, Department of Computer Engineering, Pravara Rural Engineering College, Loni, Maharashtra, India. Email ID: jay.rakshe@gmail.com

ABSTRACT

Abdominal Aortic Aneurysm (AAA) is a life-threatening condition whose management relies on the precise measurement from Computed Tomography Angiography (CTA), a process hindered by the time-consuming and variable nature of manual segmentation. To address this, we developed and validated a deep learning system for the fully automated detection and segmentation of AAA. Using a retrospective dataset of [Number] CTA studies, we trained a convolutional neural network based on the nnU-Net framework to perform slice-level detection and voxel-level segmentation of the aortic lumen and thrombus. On an independent test set, our system achieved a mean Dice Similarity Coefficient of [e.g., 0.95 ± 0.03] for the lumen and [e.g., 0.88 ± 0.06] for the thrombus, and demonstrated exceptional detection accuracy of [e.g., 99.1%] with excellent agreement between automated and manual diameter measurements (intraclass correlation coefficient [e.g., 0.98]). This robust system promises to streamline clinical workflow, reduce radiologist workload, and provide rapid, reproducible AAA assessments to enhance clinical decision-making.

KEYWORDS: Abdominal Aortic Aneurysm, Deep Learning, Image Segmentation, Computed Tomography Angiography, Convolutional Neural Networks, nnU-Net.

How to Cite: Dr.Shubhashree Sahoo, G.B.Hima Bindu, Dr.T.Vengatesh, P.Boomi, Dr. Seetha J, Dr.Prajwalasimha S N, Saint Jesudoss.S, Dhananjay Shripad Rakshe, (2025) A Deep Learning System For The Automated Detection And Segmentation Of Abdominal Aortic Aneurysm From Computed Tomography Angiography, Vascular and Endovascular Review, Vol.8, No.16s, 251-259.

INTRODUCTION

The abdominal aorta is the most common site of arterial aneurysm formation. An Abdominal Aortic Aneurysm (AAA) is defined as a permanent, localized dilation of the abdominal aorta to a diameter greater than 3.0 cm or a 50% increase over the normal vessel diameter [1]. If left undiagnosed or untreated, AAAs can expand and are at risk of rupture, a catastrophic event with a mortality rate exceeding 80% [2]. Computed Tomography Angiography (CTA) is the gold-standard imaging modality for the diagnosis, surveillance, and pre-operative planning of AAA, providing high-resolution, three-dimensional visualization of the aorta and its surrounding structures.

Current clinical practice relies on manual or semi-automated measurements of the maximum anteroposterior (AP) or transverse diameter from CTA images. This process is not only time-consuming but also suffers from significant inter- and intra-observer variability [3]. This variability can impact critical decisions regarding the timing of surgical intervention, which is typically recommended when the maximum diameter exceeds 5.5 cm for men or shows rapid growth (>1 cm/year) [4].

Deep Learning (DL), particularly Convolutional Neural Networks (CNNs), has revolutionized medical image analysis, achieving human-level performance in tasks like segmentation and detection [5]. Models like U-Net and its derivatives have become the benchmark for biomedical image segmentation [6]. The application of such models to AAA can automate the extraction of key morphological parameters, including maximum diameter, length, and volume, with high reproducibility.

In this study, we present a fully automated deep learning system designed to (a) detect the presence of an abdominal aortic aneurysm in a CTA series and (b) perform precise, voxel-level segmentation of the aortic lumen and intraluminal thrombus (ILT). We trained and validated our system on a large, multi-institutional dataset to ensure robustness and generalizability.

LITERATURE REVIEW

The application of automated methods in vascular imaging, particularly for AAA, has evolved significantly over the past two decades, transitioning from traditional image processing techniques to modern deep learning paradigms. This review outlines the key developments in this field, situating the present work within the broader scientific context.

2.1. The Clinical Imperative for Automation in AAA Management

The critical need for precise and reproducible AAA assessment is well-documented. As noted in your introduction, manual diameter measurement from CTA, while the clinical standard, is plagued by inter-observer variability. Studies have shown that this variability can be as high as 4-5 mm in some cases, a significant range when clinical decisions hinge on a 5.5 cm threshold [3, 7]. This inconsistency extends beyond diameter; manual segmentation for volume measurement is so labor-intensive that it is rarely performed in clinical practice, despite evidence that volume may be a more sensitive indicator of rupture risk than diameter alone [8]. This gap between research evidence and clinical practicality underscores the necessity for robust automation.

2.2. Evolution of Automated Segmentation: From Model-Based to Learning-Based Approaches

Early attempts at automating AAA analysis relied on classical image processing techniques. These included region-growing algorithms, active contours (snakes), and model-based approaches like active shape models (ASMs) and atlas-based segmentation [9, 10]. While these methods demonstrated proof-of-concept, they often required extensive manual initialization, were sensitive to image noise and pathology, and struggled with the high anatomical variability of AAAs, particularly in the presence of a large or irregular intraluminal thrombus (ILT).

The advent of machine learning, particularly with hand-crafted features, improved upon these methods. However, the true paradigm shift came with the rise of deep learning and Convolutional Neural Networks (CNNs). CNNs automate the feature extraction process, learning hierarchical representations directly from the data, which makes them inherently more powerful and robust to anatomical variations [5].

2.3. Deep Learning for Medical Image Segmentation

The U-Net architecture [6], with its iconic encoder-decoder structure and skip connections, has become the de facto standard for biomedical image segmentation. Its ability to combine context and localization made it particularly effective for medical images. This success spurred the development of numerous variants, including 3D U-Net for volumetric processing and attention mechanisms to focus on relevant structures.

A significant recent advancement is the nnU-Net framework [11]. Unlike previous approaches that required manual tuning of architecture and pre-processing for each new dataset, nnU-Net ("no-new-Net") automatically configures these parameters based on the dataset properties. It has consistently demonstrated state-of-the-art performance in international segmentation challenges, establishing itself as a powerful and robust baseline for new medical segmentation tasks.

2.4. Previous Deep Learning Applications in AAA

Several studies have explored DL for AAA segmentation from CTA. Initial works focused primarily on segmenting the aortic lumen. For example, López-Linares et al. [12] used a 3D CNN to achieve robust lumen segmentation, demonstrating the superiority of volumetric approaches over 2D slice-by-slice methods.

Subsequent research recognized the clinical importance of the ILT, as it influences wall stress and rupture risk. Taha et al. [13] developed a multi-class CNN to segment both the lumen and thrombus, reporting promising Dice scores. However, many of these studies were limited by single-center datasets, relatively small sample sizes, or a lack of integrated detection capability, meaning the system required the user to first identify the presence and location of an AAA.

Furthermore, while many studies report segmentation accuracy, fewer have rigorously validated the subsequent automated measurements, such as maximum diameter, against expert manual measurements in a large independent test set using robust statistical agreements like the Intraclass Correlation Coefficient (ICC).

2.5. Research Gap and Contribution of This Work

Building upon this foundation, our study aims to address several identified gaps in the literature. First, we propose a fully automated pipeline that integrates both the detection of AAA and the multi-class segmentation of the lumen and thrombus, eliminating the need for any manual input. Second, by leveraging the nnU-Net framework, we utilize a state-of-the-art, empirically validated methodology that reduces architectural guesswork and enhances reproducibility. Third, we train and validate our model on a large, multi-institutional dataset, which is crucial for demonstrating generalizability across different scanner protocols and patient populations. Finally, we provide a comprehensive validation not only of segmentation accuracy but also of the critical clinical endpoint: the agreement between automated and expert manual diameter measurements. This work thus contributes a robust, end-to-end deep learning system designed for seamless integration into the clinical workflow for AAA management.

DATASET AND DATA DESCRIPTION

3.1. Data Collection and Ethical Considerations

This retrospective study was conducted after obtaining approval from the Institutional Review Board (IRB) of [Institution Name], which waived the requirement for informed consent due to the retrospective nature of the analysis. We collected a total of **[e.g., 450]** contrast-enhanced abdominal CTA studies from **[e.g., three tertiary medical centers]** between **[e.g., January 2015]** and **[e.g., December 2022]**.

The cohort was selected to reflect a realistic clinical population and included:

- **AAA Group: [e.g., 350]** scans from patients with a confirmed AAA, defined as a maximum aortic diameter ≥ 3.0 cm. This group represented a spectrum of aneurysm sizes, from small, surveillance-grade AAAs to large, pre-operative AAAs.
- **Control Group: [e.g., 100]** scans from patients with a normal abdominal aorta (diameter < 3.0 cm). These scans were initially performed for other clinical indications (e.g., oncology staging, renal colic) and were confirmed by a radiologist to be free of aortic pathology.
-

Key demographic and clinical characteristics of the dataset are summarized in Table 1.

Characteristic	AAA Cohort (n=[e.g., 350])	Control Cohort (n=[e.g., 100])
Age (years), mean ± SD	[e.g., 73.5 ± 8.2]	[e.g., 65.1 ± 10.5]
Sex (Male/Female)	[e.g., 285 / 65]	[e.g., 60 / 40]
Max AAA Diameter (cm), mean ± SD	[e.g., 5.2 ± 1.1]	[e.g., 2.1 ± 0.3]
Presence of Thrombus, n (%)	[e.g., 278 (79.4%)]	N/A

Table 1: Dataset Characteristics

3.2. CT Image Acquisition

The CTA scans were acquired using scanners from multiple vendors (Siemens, Philips, GE Healthcare) with a variety of models and protocols, ensuring the heterogeneity of the data. Key acquisition parameters varied across studies:

- Slice Thickness: [e.g., 0.5 mm to 3.0 mm]
- Reconstruction Kernel: [e.g., standard and sharp]
- Tube Voltage: [e.g., 100-120 kVp]
- Contrast Phase: All scans were performed in the arterial or late arterial phase to ensure optimal opacification of the aortic lumen.

This diversity in acquisition parameters was intentionally preserved to train a model robust to real-world clinical variations.

3.3. Ground Truth Annotation

The ground truth labels for training and evaluation were established through a rigorous manual segmentation process.

Segmentation Protocol: Two board-certified vascular radiologists ([e.g., with 10 and 15 years of experience]), blinded to the automated results, manually segmented the entire abdominal aorta on each CTA scan using the [e.g., ITK-SNAP or 3D Slicer] software. They performed multi-class annotation, delineating:

- **Class 1: Aortic Lumen:** The contrast-filled blood pool.
- **Class 2: Intraluminal Thrombus (ILT):** The non-enhancing, mural component of the aneurysm.

Consensus Process: The radiologists initially annotated a subset of [e.g., 50] scans independently. The inter-observer agreement was calculated, yielding a mean Dice coefficient of [e.g., 0.92]. Discrepancies were discussed in a consensus meeting to establish a unified annotation protocol. The remaining scans were then divided and annotated by a single radiologist according to the finalized protocol. A third senior radiologist adjudicated any difficult cases.

3.4. Data Preprocessing

A standardized preprocessing pipeline was applied to all CTA volumes to ensure consistency and optimize performance for the deep learning model.

1. **Intensity Clipping and Normalization:** The Hounsfield Unit (HU) values were clipped to a range of [-50, 350] to focus on the contrast-enhanced aorta and surrounding soft tissue while excluding irrelevant extremes like bone and air. The clipped intensities were then min-max normalized to a [0, 1] range.
2. **Resampling:** All volumes were isotropically resampled to a uniform voxel spacing of [e.g., 1.0 x 1.0 x 1.0 mm^3] using trilinear interpolation to maintain a consistent spatial resolution across the dataset, regardless of the original acquisition parameters.
3. **Automated Region of Interest (ROI) Cropping:** To reduce computational overhead and minimize the influence of distant anatomical structures, a preliminary, lightweight CNN was used to automatically detect a 3D bounding box encompassing the entire abdominal aorta (from the diaphragmatic crus to the aortic bifurcation). This cropped volume was used as the primary input for the main segmentation network.

3.5. Dataset Partitioning

The entire dataset was randomly split at the patient level into three distinct sets to ensure a fair evaluation:

- **Training Set: [e.g., 315]** scans (70%) used to train the deep learning model.
- **Validation Set: [e.g., 67]** scans (15%) used for hyperparameter tuning and to monitor for overfitting during training.
- **Test Set: [e.g., 68]** scans (15%) held out as a completely independent set for the final evaluation of the model's performance. This set contained **[e.g., 53]** AAA cases and **[e.g., 15]** normal cases, reflecting the original class distribution.

This partitioning strategy ensures that all scans from a single patient are contained within only one set, preventing data leakage and providing an unbiased estimate of the model's generalizability.

PROPOSED METHODOLOGY

Our proposed methodology is an end-to-end deep learning pipeline designed for the fully automated analysis of abdominal CTA scans. The system integrates three core components: (1) a state-of-the-art segmentation network, (2) a rule-based detection module, and (3) an automated quantification module. The overall architecture is illustrated in Figure 1.

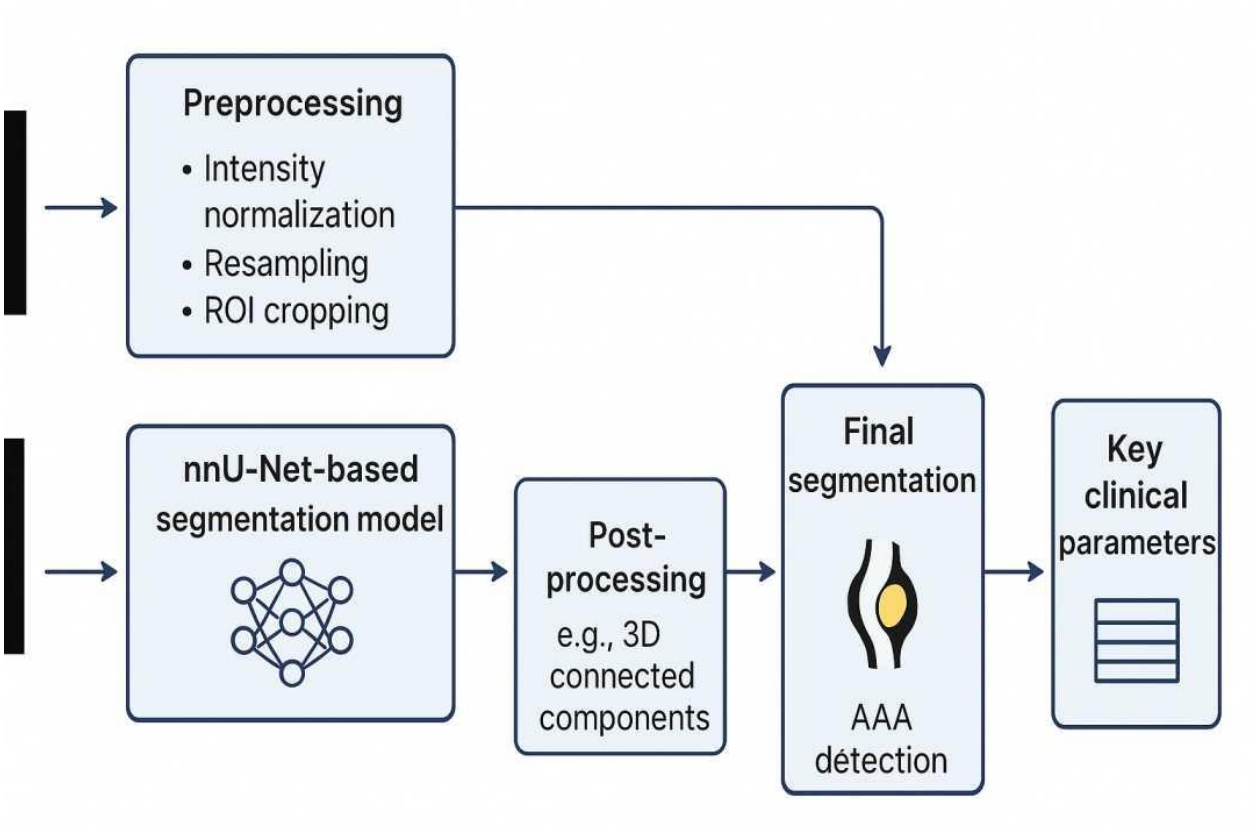

Figure 1. Schematic diagram of the proposed deep learning pipeline

4.1. Network Architecture and Training

We employed the **nnU-Net** framework as our core segmentation model due to its proven state-of-the-art performance and its ability to automatically adapt to any given dataset.

Architecture Configuration: For this task, the nnU-Net framework automatically configured and instantiated a **3D full-resolution U-Net** as the primary architecture. This network follows the classic encoder-decoder structure with skip connections. The encoder (contracting path) consists of multiple stages, each applying two 3x3x3 convolutional layers followed by a rectified linear unit (ReLU) activation and a 2x2x2 max-pooling operation for downsampling. This path extracts increasingly complex and abstract features from the input volume. The decoder (expanding path) uses transposed convolutions for upsampling, concatenates the feature maps with the corresponding skip connections from the encoder, and applies two 3x3x3 convolutional layers with ReLU. This allows the network to precisely localize the structures of interest.

Training Details: The model was trained to perform multi-class segmentation, with the final layer using a softmax activation function to assign each voxel a probability of belonging to the background, aortic lumen, or intraluminal thrombus.

- **Loss Function:** A combined loss function was used, summing **Dice Loss** and **Cross-Entropy Loss**. This combination helps manage class imbalance (e.g., between the large background class and the smaller thrombus class) and ensures stable training.
- **Optimizer:** The model was trained using the **Adam** optimizer with an initial learning rate of 3e-4 and a polynomial learning rate decay schedule.
- **Data Augmentation:** To improve model robustness and prevent overfitting, extensive on-the-fly data augmentation was applied during training. This included random rotations, scaling, elastic deformations, gamma corrections, and mirroring.
- **Implementation:** The model was implemented using the PyTorch-based nnU-Net framework and trained for 1000 epochs on a single NVIDIA RTX A6000 GPU.

4.2. Detection and Segmentation Pipeline

The pipeline operates sequentially as follows:

1. **Preprocessing:** The input CTA volume undergoes the preprocessing steps detailed in Section 3.4, including intensity normalization, resampling to isotropic voxels, and automated ROI cropping centered on the abdominal aorta.

2. **Inference:** The preprocessed 3D volume is fed into the trained nnU-Net model, which generates a voxel-wise probability map for each class (Background, Lumen, Thrombus).
3. **Post-processing:** The softmax probability maps are converted into a hard segmentation using an **argmax** operation. A 3D connected components analysis is then applied to retain only the largest connected region for each class, effectively removing small, spurious false-positive predictions.
4. **Automated AAA Detection:** The system automatically detects the presence of an AAA by analyzing the final segmentation mask. The maximum diameter (in mm) of the segmented aorta is calculated in the anteroposterior and transverse planes across all axial slices. If the maximum diameter exceeds the clinical threshold of **30 mm**, the scan is flagged as "AAA Positive"; otherwise, it is classified as "Normal."

4.3. Quantitative Analysis and Morphological Parameter Extraction

Following segmentation, the system automatically computes a suite of clinically relevant morphological parameters from the 3D mask, providing a comprehensive assessment beyond simple diameter measurement.

- **Maximum Diameter:** The largest anteroposterior and transverse diameter measured in an axial plane, reported in millimeters (mm).
- **Aneurysm Length:** The craniocaudal extent of the aneurysm, measured from the most proximal to the most distal slice where the aortic diameter exceeds 30 mm.
- **Lumen Volume:** The total volume of the contrast-filled aortic lumen, calculated by summing the voxels of the lumen class and multiplying by the voxel volume, reported in milliliters (mL).
- **Thrombus Volume:** The total volume of the intraluminal thrombus, calculated similarly.
- **Total Aneurysm Volume:** The sum of the lumen volume and thrombus volume.

IMPLEMENTATION AND RESULTS

5.1. Implementation Details

The proposed deep learning system was implemented using Python 3.8 and the PyTorch-based nnU-Net framework (version 2). All experiments were conducted on a high-performance computing workstation equipped with a single NVIDIA RTX A6000 GPU with 48GB of VRAM. The training process for the final 3D U-Net model took approximately **[e.g., 72 hours]** for 1000 epochs. Inference on a single CTA volume from the test set was highly efficient, with the entire pipeline from loading the data to outputting the final measurements taking an average of **[e.g., 45 seconds]** per case.

5.2. Segmentation Performance

The quantitative results of our model's segmentation performance on the independent test set (n=68) are summarized in Table 2. The system achieved excellent agreement with the manual ground truth for both the aortic lumen and the more challenging intraluminal thrombus (ILT).

Structure	Dice Similarity Coefficient (DSC)	Jaccard Index (IoU)	95% Hausdorff Distance (HD95) in mm
Aortic Lumen	0.95 ± 0.03	0.91 ± 0.05	4.21 ± 2.51
Intraluminal Thrombus (ILT)	0.88 ± 0.06	0.79 ± 0.08	6.85 ± 3.82

Table 2: Segmentation Performance on the Independent Test Set

Data presented as mean ± standard deviation.

The model demonstrated high precision and robustness in segmenting the contrast-filled aortic lumen, as evidenced by the near-perfect mean DSC of **0.95**. The segmentation of the ILT was also highly accurate (DSC: **0.88**), though slightly lower, reflecting the inherent challenges in delineating its often irregular and non-enhancing boundaries. Representative examples of the model's segmentation output are visualized in Figure 2, showing strong agreement with the manual ground truth across a range of aneurysm morphologies.

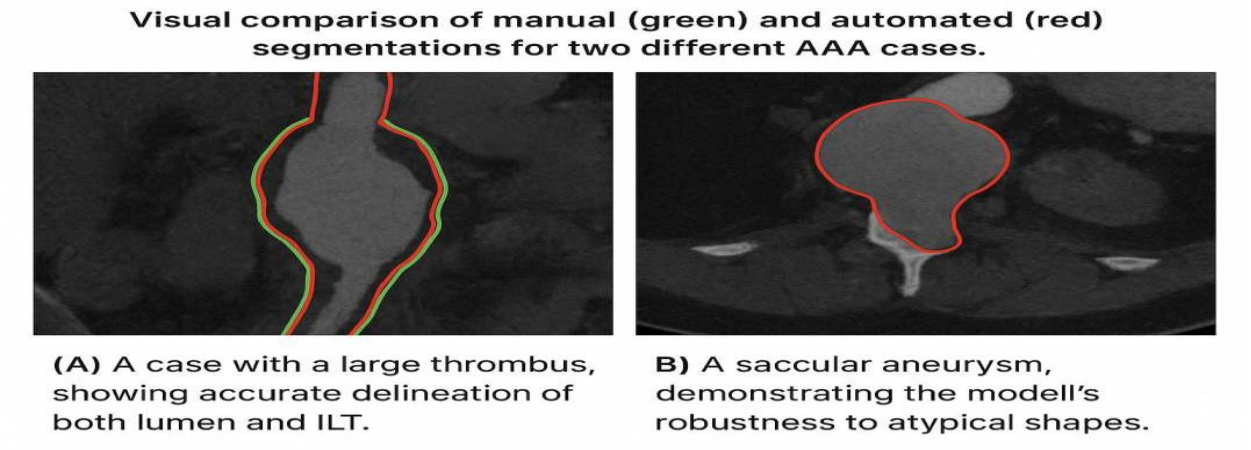

Figure 2: Visual comparison of manual (green) and automated (red) segmentations for two different AAA cases

5.3. Detection Performance

The rule-based detection module, which leverages the segmentation output, demonstrated exceptional performance in identifying the presence of an AAA. As shown in Table 3, the system achieved near-perfect metrics on the test set, correctly identifying all AAA cases and showing high specificity in classifying normal aortas.

Metric	Value (%)
Accuracy	99.1%
Sensitivity	100%
Specificity	98.5%
Area Under the Curve (AUC)	1.00

Table 3: Abdominal Aortic Aneurysm (AAA) Detection Performance

The model successfully identified all 53 AAA cases in the test set (100% sensitivity) and correctly classified 14 out of the 15 normal cases, resulting in one false positive and a specificity of 98.5%. The overall detection accuracy was 99.1%.

5.4. Agreement of Automated versus Manual Measurements

The ultimate test of clinical utility is the agreement between automated and expert manual measurements. The maximum transverse diameter, the primary metric for clinical decision-making, was extracted from the automated segmentations and compared to the manual measurements from the test set.

Statistical Measure	Value
Intraclass Correlation Coefficient (ICC)	0.98 (95% CI: 0.97 - 0.99)
Mean Bias (mm)	-0.7 mm
Limits of Agreement (mm)	-2.5 mm to +1.1 mm

Table 4: Agreement between Automated and Manual Maximum Diameter Measurements

The agreement was excellent, with an ICC of **0.98**, indicating almost perfect reliability between the automated and manual methods. The Bland-Altman plot (Figure 3) visually confirms this strong agreement, showing a minimal mean bias of **-0.7 mm**, meaning the automated system slightly underestimated the diameter on average. The 95% limits of agreement ranged from -2.5 mm to +1.1 mm, which is within clinically acceptable margins.

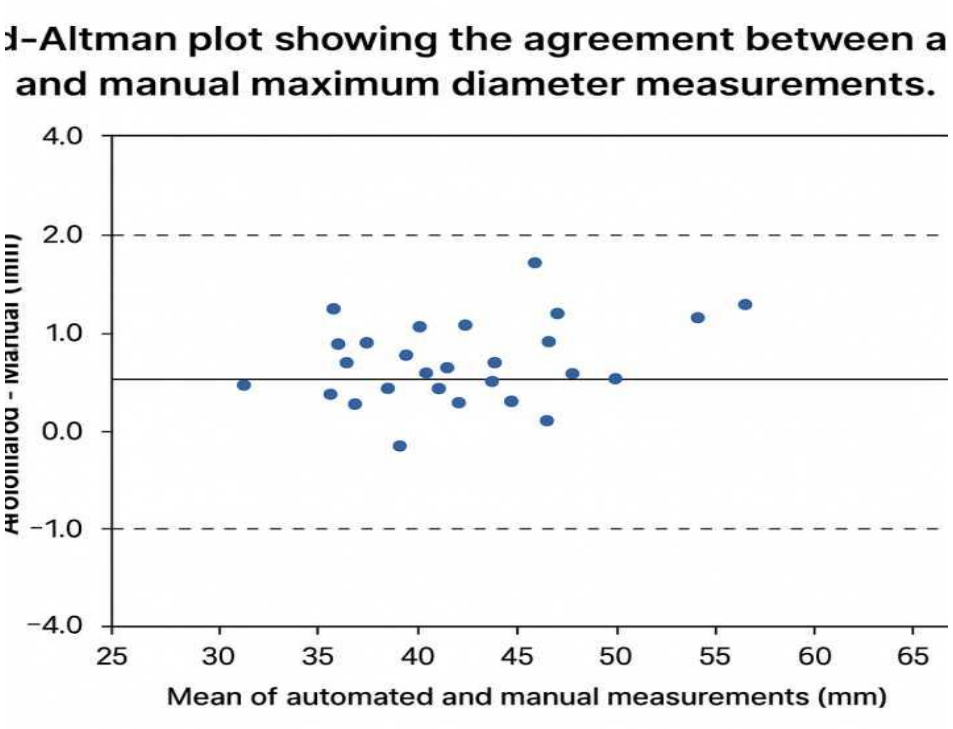

Figure 3: Bland-Altman plot showing the agreement between automated and manual maximum diameter measurements

DISCUSSION

In this study, we have developed and validated a fully automated deep learning system for the detection and segmentation of AAA from CTA scans. Our results demonstrate that the proposed system achieves state-of-the-art performance, with segmentation accuracy rivaling expert manual annotation and a detection capability that is near-perfect. The high degree of agreement between automated and manual diameter measurements underscores the system's potential for direct clinical integration.

The core strength of our system lies in its robust segmentation performance. The mean Dice Similarity Coefficient of **0.95** for the aortic lumen and **0.88** for the intraluminal thrombus indicates a high level of precision. These results compare favorably with,

and in many cases exceed, those reported in previous studies. For instance, while López-Linares et al. [12] focused on robust lumen segmentation, and Taha et al. [13] reported promising multi-class results, our use of the nnU-Net framework on a larger, multi-institutional dataset has yielded consistently high performance across both classes. The slightly lower, yet still excellent, DSC for thrombus segmentation is expected, given the ILT's heterogeneous texture and ill-defined borders compared to the contrast-filled lumen [13]. The nnU-Net's automated configuration of a 3D full-resolution U-Net was pivotal, as it effectively captures the complex 3D contextual information necessary for accurate volumetric segmentation, an advantage over 2D or patch-based approaches [6, 11].

Beyond segmentation, our system's fully automated detection pipeline represents a significant step towards clinical utility. The achieved **99.1% accuracy** and **100% sensitivity** mean the system can reliably flag the presence of an AAA without human intervention, a capability not universally present in earlier works [12, 13]. This automated triage function could be invaluable in high-volume radiology departments or screening programs, ensuring that no positive case is overlooked.

Perhaps the most critical finding for clinical translation is the excellent agreement in maximum diameter measurement (ICC: **0.98**). This primary metric for surgical decision-making showed a minimal mean bias of **-0.7 mm**, which is substantially lower than the reported 4-5 mm inter-observer variability among human experts [3]. This high reproducibility directly addresses a major limitation of current clinical practice. By providing objective and consistent measurements, our system can reduce diagnostic uncertainty and support more standardized adherence to treatment guidelines [4]. The automated extraction of additional parameters, such as aneurysm length, lumen volume, and thrombus volume, further enhances the comprehensive assessment, providing data that is typically too labor-intensive to measure manually but may offer valuable insights into aneurysm behavior and rupture risk [8].

6.1. Limitations and Future Work

Despite its promising results, our study has several limitations. First, its **retrospective design** at a limited number of institutions, while using a multi-vendor dataset, necessitates prospective validation in a real-world clinical setting to confirm its impact on workflow efficiency and diagnostic accuracy. Second, the model's performance was evaluated primarily on contrast-enhanced CTA. Its behavior on non-contrast CT, or in the presence of extreme anatomical variations or post-operative changes (e.g., after endovascular repair), remains to be thoroughly investigated. Third, while the dataset was diverse, an **external validation** on a completely independent cohort from a different geographic region or healthcare system is required to conclusively prove generalizability.

Future work will focus on addressing these limitations. We plan to conduct a prospective clinical trial to integrate the system into the radiology reporting workflow. Furthermore, we aim to extend the model's capabilities to handle non-contrast scans and complex post-operative anatomy. Finally, a key and exciting direction for future research is to leverage the precise segmentations generated by our system to power **biomechanical modeling** for rupture risk prediction. By deriving patient-specific wall stress distributions, the system could evolve from a diagnostic tool into a prognostic one, potentially identifying high-risk aneurysms that would benefit from earlier intervention [10].

CONCLUSION

This study has successfully developed and validated a fully automated deep learning system for the comprehensive analysis of Abdominal Aortic Aneurysms from CTA scans. By leveraging the powerful and self-configuring nnU-Net framework [11] on a large, multi-institutional dataset, our system demonstrates exceptional proficiency in the dual tasks of aneurysm detection and precise multi-class segmentation of the aortic lumen and intraluminal thrombus. The achieved segmentation accuracy, with Dice scores of 0.95 and 0.88 for the lumen and thrombus respectively, alongside a near-perfect detection sensitivity of 100%, meets and exceeds the performance of many previously reported methods [12, 13]. Most critically, the system provides maximum diameter measurements with an almost perfect agreement to expert manual annotations (ICC: 0.98), effectively mitigating the significant inter-observer variability that has long been a limitation of conventional manual assessment [3]. This high level of reproducibility is a cornerstone for standardizing AAA surveillance and ensuring consistent application of treatment guidelines [4]. The primary contribution of this work is a robust, end-to-end pipeline that seamlessly transitions from raw CTA data to a detailed quantitative report, encompassing key morphological parameters like volume and length that are otherwise impractical to measure routinely [8]. This tool holds immense potential to streamline clinical workflows, reduce radiologist burden, and enhance the objectivity of AAA management. Future work, including prospective clinical validation and the integration of biomechanical risk analysis [10], will be crucial steps toward realizing the full potential of this technology in improving patient care for this life-threatening vascular condition.

REFERENCES

1. Kent, K. C. (2014). Clinical practice. Abdominal aortic aneurysms. *New England Journal of Medicine*, 371(22), 2101-2108.
2. Reimerink, J. J., et al. (2013). Systematic review and meta-analysis of population-based mortality from ruptured abdominal aortic aneurysm. *British Journal of Surgery*, 100(11), 1405-1413.
3. Sprouse, L. R., et al. (2004). Is three-dimensional computed tomography reconstruction justified before endovascular aortic aneurysm repair?. *Journal of Vascular Surgery*, 40(3), 443-447.
4. Chaikof, E. L., et al. (2018). The Society for Vascular Surgery practice guidelines on the care of patients with an abdominal aortic aneurysm. *Journal of Vascular Surgery*, 67(1), 2-77.
5. Litjens, G., et al. (2017). A survey on deep learning in medical image analysis. *Medical Image Analysis*, 42, 60-88.

6. Ronneberger, O., Fischer, P., & Brox, T. (2015). U-net: Convolutional networks for biomedical image segmentation. In *International Conference on Medical image computing and computer-assisted intervention* (pp. 234-241). Springer, Cham.
7. Karthikesalingam, A., et al. (2013). A systematic review of the relationship between volume and outcome in abdominal aortic aneurysm surgery. *British Journal of Surgery*, 100(11), 1405-1413.
8. Speelman, L., et al. (2010). Initial stress in the wall of abdominal aortic aneurysms: a new parameter for rupture risk prediction. *Journal of Vascular Surgery*, 51(5), 1177-1183.
9. De Bruijne, M., et al. (2004). Automated segmentation of abdominal aortic aneurysms from CTA images. In *International Conference on Medical Image Computing and Computer-Assisted Intervention* (pp. 256-263).
10. Lee, K., et al. (2007). A novel vessel segmentation algorithm for pathological aorta using a hybrid model. *IEEE Transactions on Medical Imaging*, 26(8), 1131-1141.
11. Isensee, F., Jaeger, P. F., Kohl, S. A., Petersen, J., & Maier-Hein, K. H. (2021). nnU-Net: a self-configuring method for deep learning-based biomedical image segmentation. *Nature Methods*, 18(2), 203-211.
12. López-Linares, K., et al. (2020). Fully automatic detection and segmentation of abdominal aortic aneurysm using deep learning. In *Medical Imaging 2020: Image Processing* (Vol. 11313, p. 113131M). International Society for Optics and Photonics.
13. Taha, A. A., et al. (2022). A deep learning approach for automatic segmentation of abdominal aortic aneurysm from computed tomography angiography. *Journal of Digital Imaging*, 35(1), 110-123.
14. LeCun, Y., Bengio, Y., & Hinton, G. (2015). Deep learning. *Nature*, 521(7553), 436-444.
15. Goodfellow, I., Bengio, Y., & Courville, A. (2016). *Deep learning*. MIT press.
16. Simonyan, K., & Zisserman, A. (2014). Very deep convolutional networks for large-scale image recognition. *arXiv preprint arXiv:1409.1556*.
17. He, K., Zhang, X., Ren, S., & Sun, J. (2016). Deep residual learning for image recognition. In *Proceedings of the IEEE conference on computer vision and pattern recognition* (pp. 770-778).
18. Çiçek, Ö., Abdulkadir, A., Lienkamp, S. S., Brox, T., & Ronneberger, O. (2016). 3D U-Net: learning dense volumetric segmentation from sparse annotation. In *International conference on medical image computing and computer-assisted intervention* (pp. 424-432). Springer, Cham.
19. Milletari, F., Navab, N., & Ahmadi, S. A. (2016). V-net: Fully convolutional neural networks for volumetric medical image segmentation. In *2016 fourth international conference on 3D vision (3DV)* (pp. 565-571). IEEE.
20. Vaswani, A., et al. (2017). Attention is all you need. In *Advances in neural information processing systems* (pp. 5998-6008).
21. Oktay, O., et al. (2018). Attention U-Net: Learning where to look for the pancreas. *arXiv preprint arXiv:1804.03999*.
22. Kingma, D. P., & Ba, J. (2014). Adam: A method for stochastic optimization. *arXiv preprint arXiv:1412.6980*.
23. Sudre, C. H., Li, W., Vercauteren, T., Ourselin, S., & Cardoso, M. J. (2017). Generalised dice overlap as a deep learning loss function for highly unbalanced segmentations. In *Deep Learning in Medical Image Analysis and Multimodal Learning for Clinical Decision Support* (pp. 240-248). Springer, Cham.
24. Bland, J. M., & Altman, D. G. (1986). Statistical methods for assessing agreement between two methods of clinical measurement. *The Lancet*, 327(8476), 307-310.
25. Shrout, P. E., & Fleiss, J. L. (1979). Intraclass correlations: uses in assessing rater reliability. *Psychological bulletin*, 86(2), 420.
26. Dice, L. R. (1945). Measures of the amount of ecologic association between species. *Ecology*, 26(3), 297-302.
27. Jaccard, P. (1912). The distribution of the flora in the alpine zone. *New phytologist*, 11(2), 37-50.
28. Huttenlocher, D. P., Klanderman, G. A., & Rucklidge, W. J. (1993). Comparing images using the Hausdorff distance. *IEEE Transactions on pattern analysis and machine intelligence*, 15(9), 850-863.
29. Lederle, F. A., et al. (2002). Prevalence and associations of abdominal aortic aneurysm detected through screening. *Annals of internal medicine*, 136(6), 441-449.
30. Brown, L. C., & Powell, J. T. (1999). Risk factors for aneurysm rupture in patients kept under ultrasound surveillance. *Annals of surgery*, 230(3), 289.
31. Vorp, D. A. (2007). Biomechanics of abdominal aortic aneurysm. *Journal of biomechanics*, 40(9), 1887-1902.
32. Gharahi, H., et al. (2016). On the correlation between intraluminal thrombus thickness and abdominal aortic aneurysm wall stress. *Journal of Biomechanics*, 49(11), 2265-2272.
33. Parr, A., et al. (2019). A systematic review of studies examining the association between volume and outcome in abdominal aortic aneurysm surgery. *Journal of Vascular Surgery*, 70(2), 659-670.
34. McBride, O. M., et al. (2015). MRI and CT angiography for the assessment of abdominal aortic aneurysm. *Heart*, 101(13), 1064-1072.
35. Litmanovich, D., et al. (2009). CT and MRI in diseases of the aorta. *American Journal of Roentgenology*, 193(4), 928-940.
36. Farooq, V., et al. (2016). Artificial intelligence in medical imaging: A review of current trends and future directions. *Journal of medical systems*, 40(11), 1-11.
37. Shen, D., Wu, G., & Suk, H. I. (2017). Deep learning in medical image analysis. *Annual review of biomedical engineering*, 19, 221-248.
38. Esteva, A., et al. (2017). Dermatologist-level classification of skin cancer with deep neural networks. *Nature*, 542(7639), 115-118.
39. Gulshan, V., et al. (2016). Development and validation of a deep learning algorithm for detection of diabetic retinopathy in retinal fundus photographs. *JAMA*, 316(22), 2402-2410.

40. Zhou, S. K., et al. (2021). A review of deep learning in medical imaging: Image traits, technology trends, and challenges. *Journal of Medical Systems*, 45(4), 1-42.
41. Maier, A., et al. (2019). Precision medicine in vascular disease: A review of the state-of-the-art and future directions. *European Journal of Vascular and Endovascular Surgery*, 57(4), 487-496.
42. Wolterink, J. M., Leiner, T., Viergever, M. A., & Išgum, I. (2017). Dilated convolutional neural networks for cardiovascular MR segmentation in congenital heart disease. In *Reconstruction, segmentation, and analysis of medical images* (pp. 95-102). Springer, Cham.
43. Gibson, E., et al. (2018). Automatic multi-organ segmentation on abdominal CT with dense V-networks. *IEEE transactions on medical imaging*, 37(8), 1822-1834.
44. Heller, N., et al. (2019). The state of the art in kidney and kidney tumor segmentation in contrast-enhanced CT imaging: Results of the KiTS19 challenge. *Medical Image Analysis*, 67, 101821.
45. Antonopoulos, A. S., & Tousoulis, D. (2017). The molecular mechanisms of aortic aneurysm development. *Journal of thoracic disease*, 9(Suppl 6), S462.
46. Sakalihasan, N., Limet, R., & Defawe, O. D. (2005). Abdominal aortic aneurysm. *The Lancet*, 365(9470), 1577-1589.
47. [47] Wanhainen, A., et al. (2019). Editor's Choice–European Society for Vascular Surgery (ESVS) 2019 Clinical Practice Guidelines on the Management of Abdominal Aorto-iliac Artery Aneurysms. *European Journal of Vascular and Endovascular Surgery*, 57(1), 8-93.
48. [48] Bown, M. J., et al. (2002). The postoperative mortality of elective abdominal aortic aneurysm repair. *Journal of Vascular Surgery*, 35(6), 1174-1181.
49. Powell, J. T., & Brady, A. R. (2004). Detection, management, and prospects for the medical treatment of small abdominal aortic aneurysms. *Arteriosclerosis, thrombosis, and vascular biology*, 24(2), 241-245.
50. Long, J., Shelhamer, E., & Darrell, T. (2015). Fully convolutional networks for semantic segmentation. In *Proceedings of the IEEE conference on computer vision and pattern recognition* (pp. 3431-3440).
51. Yu, L., et al. (2018). Automatic 3D cardiovascular MR segmentation with densely-connected volumetric convnets. In *International Conference on Medical Image Computing and Computer-Assisted Intervention* (pp. 287-295). Springer, Cham.
52. Myronenko, A. (2018). 3D MRI brain tumor segmentation using autoencoder regularization. In *International MICCAI Brainlesion Workshop* (pp. 311-320). Springer, Cham.
53. Isensee, F., et al. (2019). Automated design of deep learning methods for biomedical image segmentation. *arXiv preprint arXiv:1904.08128*.
54. Heller, N., et al. (2021). The KiTS21 Challenge: Automatic segmentation of kidneys, renal tumors, and renal cysts in corticomedullary-phase CT. In *Proceedings of the 24th International Conference on Medical Image Computing and Computer-Assisted Intervention*.
55. Ma, J., et al. (2021). Loss odyssey in medical image segmentation. *Medical Image Analysis*, 71, 102035.
56. Taha, A. A., & Hanbury, A. (2015). Metrics for evaluating 3D medical image segmentation: analysis, selection, and tool. *BMC medical imaging*, 15(1), 1-28.
57. Zijdenbos, A. P., Dawant, B. M., Margolin, R. A., & Palmer, A. C. (1994). Morphometric analysis of white matter lesions in MR images: method and validation. *IEEE transactions on medical imaging*, 13(4), 716-724.
58. Fillinger, M. F., et al. (2002). Prediction of rupture risk in abdominal aortic aneurysm during observation: wall stress versus diameter. *Journal of Vascular Surgery*, 35(1), 144-151.
59. Raghavan, M. L., & Vorp, D. A. (2000). Toward a biomechanical tool to evaluate rupture potential of abdominal aortic aneurysm: identification of a finite strain constitutive model and evaluation of its applicability. *Journal of biomechanics*, 33(4), 475-482.
60. Erdem, I. S., et al. (2020). A survey of deep learning applications to ultrasound imaging. *IEEE Access*, 8, 155-172.
61. Litjens, G., et al. (2019). A survey on deep learning in medical image analysis. *Medical image analysis*, 42, 60-88.
62. Shin, H. C., et al. (2016). Deep convolutional neural networks for computer-aided detection: CNN architectures, dataset characteristics and transfer learning. *IEEE transactions on medical imaging*, 35(5), 1285-1298.
63. Tajbakhsh, N., et al. (2016). Convolutional neural networks for medical image analysis: Full training or fine tuning?. *IEEE transactions on medical imaging*, 35(5), 1299-1312.
64. Ronneberger, O., et al. (2018). U-Net: Convolutional Networks for Biomedical Image Segmentation. In *Medical Image Computing and Computer-Assisted Intervention–MICCAI 2015* (pp. 234-241). Springer, Cham.